ELSEVIER

Recent advances in graphene quantum dots for sensing

Hanjun Sun[1,2], Li Wu[1,2], Weili Wei[1] and Xiaogang Qu[1,*]

[1] Laboratory of Chemical Biology, Division of Biological Inorganic Chemistry, State Key Laboratory of Rare Earth Resource Utilization, Changchun Institute of Applied Chemistry, Chinese Academy of Sciences, Changchun 130022, PR China
[2] University of Chinese Academy of Sciences, Beijing 100039, PR China

Graphene quantum dots (GQDs) are a kind of 0D material with characteristics derived from both graphene and carbon dots (CDs). Combining the structure of graphene with the quantum confinement and edge effects of CDs, GQDs possess unique properties. In this review, we focus on the application of GQDs in electronic, photoluminescence, electrochemical and electrochemiluminescence sensor fabrication, and address the advantages of GQDs on physical analysis, chemical analysis and bioanalysis. We have summarized different techniques and given future perspectives for developing smart sensing based on GQDs.

Introduction

Graphene quantum dots (GQDs), as defined, are a kind of 0D material with characteristics derived from both graphene and CDs, which can be regarded as incredibly small pieces of graphene [1–4]. By converting 2D graphene sheets into 0D GQDs, the GQDs exhibit new phenomena due to quantum confinement and edge effects, which are similar to CDs [4]. Compared with organic dyes and semiconductive quantum dots (QDs), GQDs are superior in terms of their excellent properties, such as high photostability against photobleaching and blinking, biocompatibility, and low toxicity [1,2,4]. Unlike their cousins, CDs, GQDs clearly possess a graphene structure inside the dots, regardless of the dot size, which endows them with some of the unusual properties of graphene [3,4]. For these reasons, GQDs have attracted significant attention from researchers.

In the early research on GQDs, tremendous effort was devoted to developing methods for the preparation of GQDs and exploring their properties [1–4]. Their application in the analytical field has not been explored until very recently. Due to their novel properties, sensors based on GQDs can achieve a high level of performance. In this review, we primarily focus on sensors and analytical systems that utilize GQDs as a key component (Fig. 1). We hope this review will offer some important perspectives and expand the applications of GQDs for sensing in the future.

*Corresponding author:. Qu, X. (xqu@ciac.ac.cn)

Fundamentals

The preparation methods of GQDs can be classified into two categories: top–down and bottom–up methods. The strategy of top–down methods is to cut down large graphene sheets, carbon nanotubes, carbon fibers or graphite into small pieces of graphene sheet, while in the bottom–up methods, small molecules are used as starting materials to build the GQDs. Until now, for top–down approaches, nanolithography technique [5–9], acidic oxidation [10,11], hydrothermal or solvothermal [12–15] microwave-assisted [16,17], sonication-assisted [18], electrochemical [19–22], photo-Fenton reaction [23], selective plasma oxidation [24] and chemical exfoliation [25,26] methods have been used to synthesize GQDs; while for the bottom–up techniques, using benzene derivatives as starting materials through stepwise solution chemistry methods [27–29], carbonization as starting materials through microwave-assisted hydrothermal method [30,31], fullerenes as starting materials through ruthenium-catalyzed cage-opening [32] and unsubstituted hexaperihexabenzocoronene as starting materials through the process of carbonization, oxidization, surface functionalization, and reduction successively [33] have been utilized to prepare GQDs successfully. The dimensions and heights of graphene sheets in the obtained GQDs range from 1.5 to 100 nm and 0.5 to 5 nm, respectively. On the whole, the sizes of most GQDs range from 3 to 20 nm and they consist of no more than 5 layers of graphene sheets (ca. 2.5 nm) [1–4]. The shape of most GQDs is circular and elliptical, but there are triangular,

1369-7021/06/$ - see front matter http://dx.doi.org/10.1016/j.mattod.2013.10.020

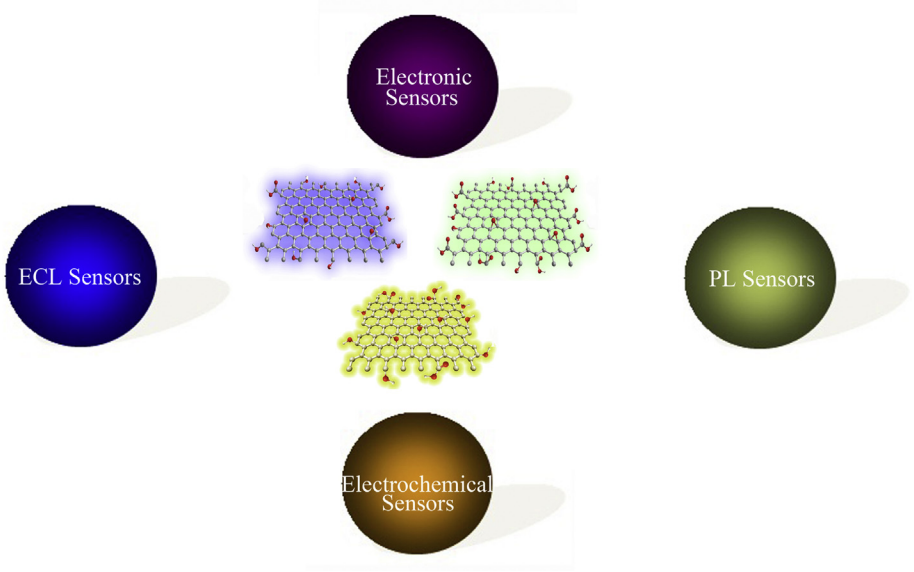

FIGURE 1

Applications of graphene quantum dots in sensors.

quadrate and hexagonal dots as well [10,34]. Generally, the composite elements (C, O and H) and the surface groups (carbonyl, carboxyl, hydroxyl and epoxy groups) of GQDs are similar to graphene [1–4]. Moreover, all the results obtained from X-ray diffraction patterns, Raman spectroscopy and high resolution transmission electron microscopy demonstrate the GQDs have a similar crystalline nature to graphene [1–4].

Electronic sensors

Unlike the extensive applications of graphene in field-effect transistor, GQDs are mainly used in single electron transistor (SET) based charge sensors [6–9]. SETs are a new type of switching device that use controlled electron tunneling to amplify a current [35]. Generally, as shown in Fig. 2, building a GQDs-based SET requires electron beam lithography carving, or oxygen reactive ion etching of the pattern-protected large graphene flakes, leading to the formation of GQDs with the desired geometries as an island. When both the gate and the bias voltages are zero, electrons did not have enough energy to enter the island and current will not flow. As the bias voltage between the source and drain is increased, an electron can pass through the island, current flows, and the detection of charge realized [6–9].

Besides detecting charge in SETs, GQDs have also been recruited to build electronic sensors for the detection of humidity and pressure [36]. As shown in Fig. 3, GQDs (ca. 100–200 nm) selectively interfaced with polyelectrolyte microfibers (diameter = 2–20 μm) form an electrically percolating-network exhibiting a characteristic Coulomb blockade signature with a dry tunneling distance of 0.58 nm and conduction activation energy of 3 meV. This construct demonstrates the functions of humidity and pressure

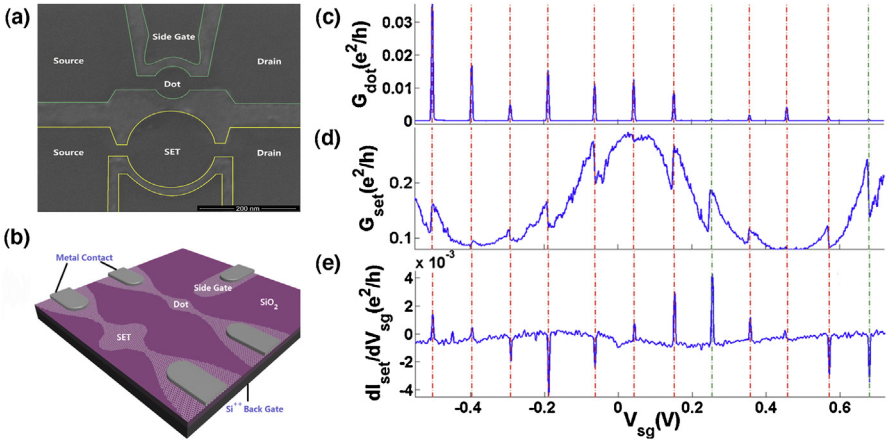

FIGURE 2

(a) Scanning electron microscope image of an etched sample structure. The scale bar has a length of 200 nm, (b) schematic of a representative device, (c) conductance through the quantum dot vs. the side gate voltage, (d) an example of conductance through the single electron transistor for the same parameter range shown in panel (c), and (e) transconductance of a single electron transistor for the same parameters as in panel (a). Reprinted with permission from [6]. © 2010 the American Institute of Physics.

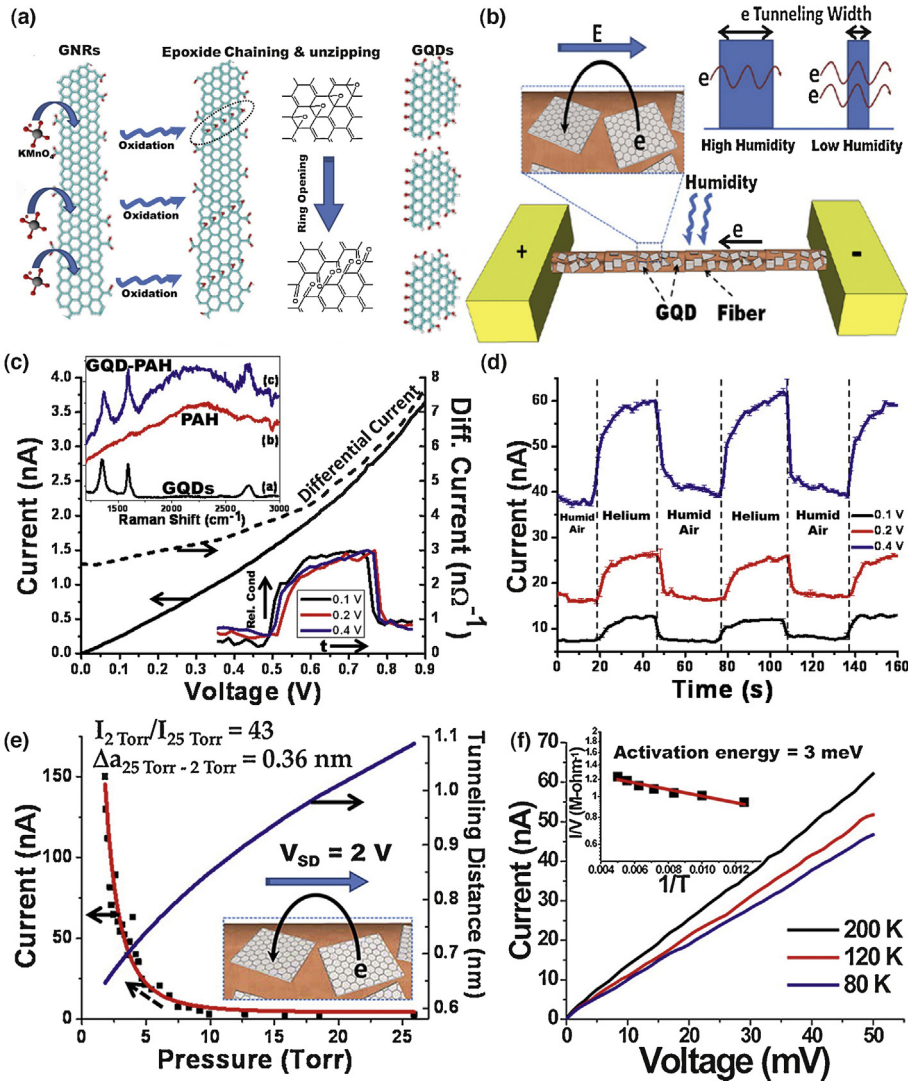

FIGURE 3

(a) Schematic representation of the conversion from graphene nanoribbons (GNRs) to GQDs, (b) schematic representation of the device construction and the mechanism employed, (c) current–voltage (*I–V*) behavior of a polyallylmine hydrochloride (PAH)–GQD device. Inset: Raman spectra of the PAH–GQD, PAH, and GQDs. The transient response of the current in the PAH–GQD device changed in response to the local humidity (d) and in different pressures at 2 V bias (e) and (f) the influence of temperature on the electrical current in the percolating-GQD device. The insert shows the activation energy was 3 meV. Reprinted with permission from [36]. © 2013 The American Chemical Society.

sensing and outlines their governing models. A 0.36 nm decrease in the average tunneling-barrier width between GQDs (tunneling barrier = 5.11 eV) increased the conductivity of the device by 43-fold. These devices use the modulation in electron tunneling distances caused by pressure and humidity induced water transport across the hygroscopic polymer microfiber (Henry's constant = 0.215 $Torr^{-1}$). Compared with traditional graphene-based sensors, the GQD-network device exhibits one order of magnitude higher current modulation (43-fold). Moreover, the device operates under a lower humidity range: 0–40% rH (<0.007 kg/kg) and the conduction increases according to the reduction in humidity – which could permit low humidity detection [36].

Photoluminescence (PL) sensors

GQDs prepared through different methods can emit photoluminescence (PL) with different colors. Up to now, deep UV [30], blue [10,12,13,16–18,23,25,26,37–39], green [10,11,13,14,16,19,25], yellow [10,11,13,21] and red [29] PL of GQDs have been reported, and the blue and green PL of GQDs are relatively common. The PL of GQDs are dominated by many factors, such as size [10,11,30], shape [34], excitation wavelength [10,33,37], pH [12,14], concentration [14,17], surface oxidation degree [16,38], surface functionalization [13,39], N-doping [20,40,41] and S-doping [42]. Similar to CDs, the PL mechanism of GQDs remains controversial. Generally, the PL of GQDs may be derived from intrinsic state emission and defect state emission [3,4]. The intrinsic state emission is induced by the quantum size effect [19], zigzag edge sites [10,12,43] or recombination of localized electron–hole pairs [44,45], and the defect state emission originates from defect effect (energy traps) [12,23].

In view of the GQDs' photoluminescence properties, GQDs have been exploited to detect many analytes [37,46–55]. The first

PL sensor based on GQDs was developed by Jin *et al.* in 2012 [46]. They found the fluorescence of GQDs synthesized by periodic acid oxidizes could be selectively quenched by Fe^{3+} ions sensitively and selectively through the charge transfer (CT) processes. Not only cations; anions can be detected by GQD PL sensors as well. Chi *et al.* made use of strong oxidative free chlorine that can destroy the surface passivation layer of GQDs prepared by pyrolyzing citric acid, leading to significant PL quenching, and developed a sensitive, selective, rapid, facile, and particularly green sensor to detect free chlorine in drinking water [47]. Moreover, some organic molecules with aromatic structures have a strong interaction with GQDs through the electrostatic interaction, π–π stacking or hydrogen bonding, resulting in the energy transfer or luminescence resonance energy transfer (LRET) [37,48]. The PL quenching caused by these organic molecules was also used to design PL sensors. Wang *et al.* utilized the PL quenching arising from the π–π stacking between TNT and GQDs, achieving sensitive TNT detection [48]. Yang *et al.* found that the PL intensity of GQDs decreased with the increasing concentration of pyrocatechol [37]. They stated that the oxygen-containing groups in GQDs enabled electrostatic interaction, π–π stacking or hydrogen bonding interaction between GQDs and pyrocatechol, leading to the energy transfer and further the PL quenching of the GQDs.

Apart from the *signal-off* PL sensors described above, some *signal-on* PL sensors have been designed as well [49–51]. Qiu *et al.* presented a PL sensor for phosphate (Pi) sensing with GQDs as an effective sensing platform [49]. This system was a combination of GQDs and Eu^{3+} ions which could coordinate to the carboxylate groups on the surface of the GQDs, acting as a bridge for the induction of GQD aggregation. When treated with Eu^{3+} ions, the PL of GQDs was quenched (signal off) through energy-transfer or electron-transfer processes. The GQD aggregates could be dissociated after the introduction of Pi because Eu^{3+} ions displayed a higher affinity to the oxygen-donor atoms in Pi than the carboxylate groups on the GQD surface. The subsequent redispersion of GQDs results in the restoration of PL (signal on) (Fig. 4a). Moreover, a novel glucose sensing system operating under physiological conditions was designed using anionic fluorescent GQDs that bear polar surface groups of carboxyl and hydroxyl, and a cationic boronic acid-substituted bipyridinium salt (BBV) by Qiu's group [50]. In this sensor, pristine GQDs acted as a fluorescent reporting unit, and BBV served as a fluorescence quencher and a glucose receptor simultaneously. It was postulated that electrostatic attraction between GQDs and BBV resulted in the formation of a ground-state complex which facilitated the excited-state electron transfer (ET) from GQDs to bipyridinium, leading to a decrease in the PL intensity of the GQDs. When treated with glucose, the boronic acids were converted to tetrahedral anionic glucoboronate esters, which effectively neutralized the net charge of the cationic bipyridinium, thus greatly diminishing its quenching efficiency,

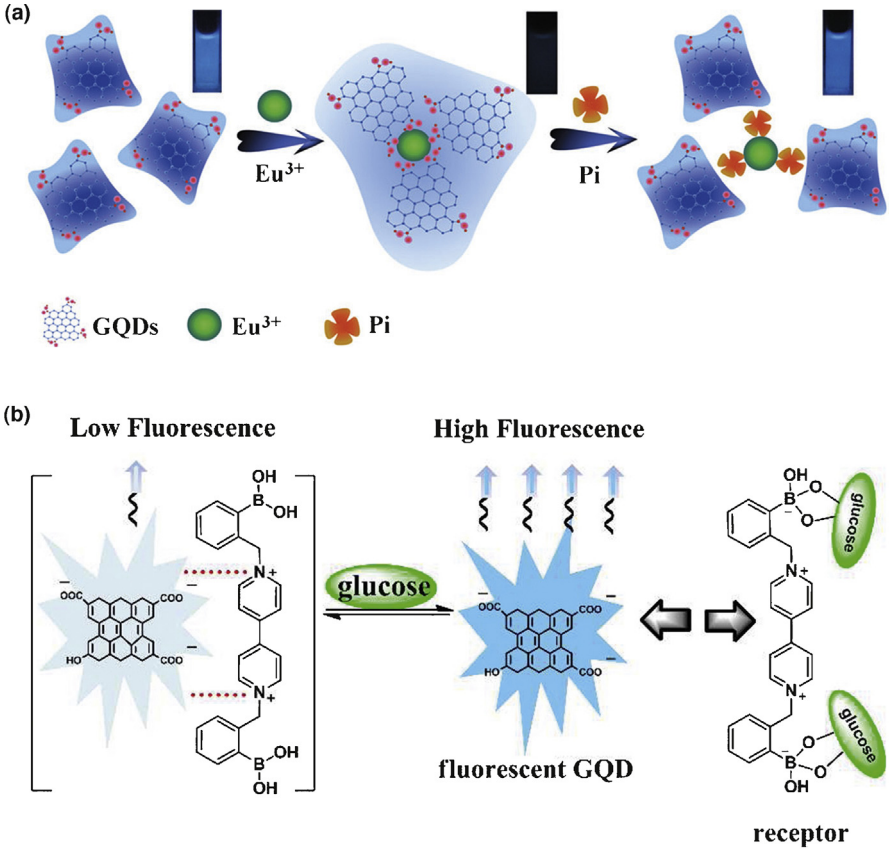

FIGURE 4

(a) Schematic illustration of Pi detection based on the competition between Pi and carboxylate groups on the GQDs surface for Eu^{3+} ions. Reprinted with permission from [49]. © 2013 Wiley-VCH Verlag GmbH & Co. KGaA and (b) proposed glucose-sensing mechanism based on BBV receptor and fluorescent GQDs. Reprinted with permission from [50]. © 2013 The Royal Society of Chemistry.

and the PL intensity of the GQDs recovered. Taking advantage of the observed PL change, the fast, sensitive and selective detection of glucose was realized (Fig. 4b). Chen and co-workers developed a facile pyrolysis approach for the preparation of GQDs@glutathione (GSH) with a fluorescence quantum yield as high as 33.6%. Fe^{3+} could quench the fluorescence of GQDs@GSH by ET and then were disassociated from GQDs@GSH by the phosphate ions through the strong interactions, so that the fluorescence turned on. On the basis of the fluorescence ''off-to-on'' mechanism of GQDs@GSH, they proposed a simple method for the assay of phosphate-containing molecules. As for ATP, a sensitive detection limit of 22 μM was obtained. In addition, since ATP is the major phosphate-containing metabolite in cell lysates and blood serum, the proposed sensing approach was successfully applied to estimate the ATP level in cell lysates and human blood serum [51].

Considering the similarity between GQDs and graphene, it is natural to expect to take advantage of some of graphene's properties, and some facile PL sensors of GQDs have been designed [52,53]. Inspired by the phenomena that noble metal precursors could be reduced by graphene sheets, and that the fluorescence of GQDs can be quenched by the metal clusters or nanoparticles formed by ions through CT processes, we designed a sensor to detect Ag^{+} through the quenching effect of the formation of Ag nanoparticles on GQDs; meanwhile, since thiols have been reported to form Ag–S bonds on the surface of Ag nanoparticles (AgNPs), biothiol detection could also be realized (Fig. 5a). Since the GQDs' structure is similar to that of graphene, the π–π stacking between graphene and GQDs can bring them into LRET proximity, thus leading to the luminescence quenching of GQDs by graphene [52]. Zhao *et al.* presented a universal signaling transduction strategy in the fluoroimmunoassay based on the regulation of the interaction between graphene and GQDs, and explored its application in immunoglobulin G (IgG) sensing (Fig. 5b) [53].

Like CDs and graphene, GQDs appear to have low toxicity which makes them a promising material for biology and medical imaging [1–4]. Considering the photostability and low toxicity of GQDs, GQDs are also used in some intercellular sensors [39,54]. Dong *et al.* synthesized Au nanocube@SiO_2@GQDs hybrid nanocomposites which involved the synthesis of Au nanocubes (Au NCs), SiO_2 shell modification, and the final self-assembly of GQDs onto the particle surfaces [54]. The mesoporous silica shells provided a dielectric spacer between the GQDs and AuNCs, and spatially separated GQDs on the AuNCs surface. The fluorescent enhancement and photostability improvement was observed from AuNCs@SiO_2@GQDs compared with that of pure GQDs in aqueous solution, which is mainly due to the local electric field amplification. The synthesized nanocomposites were successfully used as fluorescence probes for the selective imaging of membrane-bound proteins under living cell conditions. Very recently, our group reported a new kind of fluorescent probe for both Cu^{2+} recognition and signal generation based on GQDs [39]. As shown in Fig. 6, the amino-functionalized GQDs (afGQDs) were synthesized through the hydrothermal amination of GQDs. Compared with greenish yellow fluorescent GQDs (gGQDs), both the PL quantum yield (QY) of GQDs and selectivity to Cu^{2+} improved, and conversion of the surface charge to positive makes the cellular uptake of GQDs easier. Using afGQDs as a fluorescence probe, the profiling of Cu^{2+} in living cells was successfully realized [39].

Electrochemical sensors

Taking advantage of the electrochemical properties similar to graphene, GQDs are widely used as a kind of novel electrode material, not only in fuel cells [20,28,56], supercapacities [57,58], and photovoltaic cells [19,29,59], but also in the field of electrochemical sensors [60–63]. Furthermore, GQDs of tunable sizes 2.2 ± 0.3, 2.6 ± 0.2, and 3 ± 0.3 nm can act as multivalent

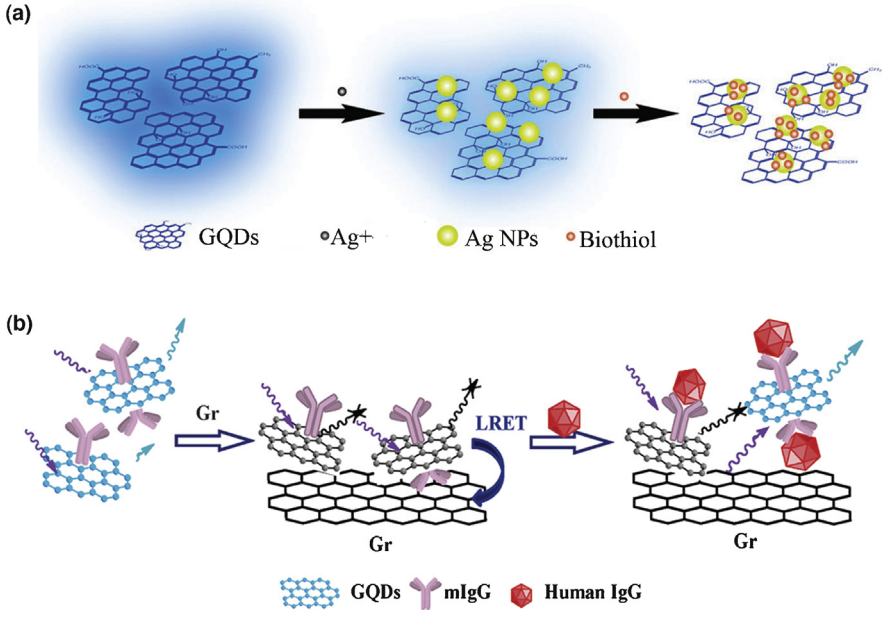

FIGURE 5

(a) Schematic illustration of the mechanism of Ag+ and biothiol detection based on graphene quantum dots. Reprinted with permission from [52]. © 2013 The Royal Society of Chemistry and (b) schematic illustration of a universal immunosensing strategy based on the regulation of the interaction between graphene and GQDs. Reprinted with permission from [53]. © 2013 The Royal Society of Chemistry.

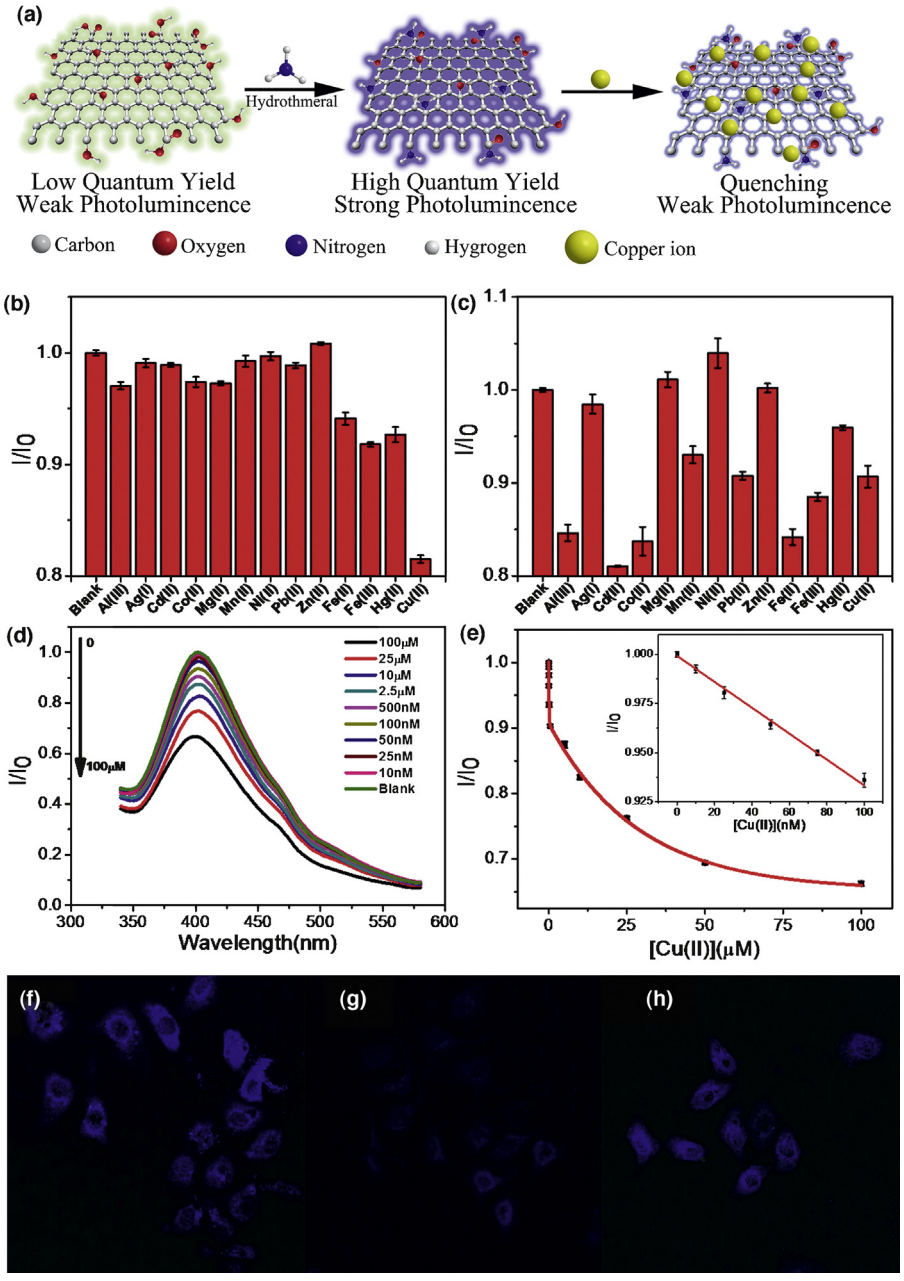

FIGURE 6

(a) Schematic representation of the preparation route for afGQDs and its quenching effect by copper ions. Selectivity of the metal ions (10 μM) based on the afGQDs (b) and gGQDs (c), (d) PL spectra of afGQDs in the presence of increasing Cu^{2+} concentrations (0–100 μM), (e) the relationship between PL of afGQDs and [Cu^{2+}]. Washed cells imaged without Cu^{2+} (f); with Cu^{2+} (10 μM) (g); with Fe^{3+} (10 μM) (h) in dark field. Reprinted with permission from [39]. © 2013 Wiley-VCH Verlag GmbH & Co. KGaA.

redox species using cyclic voltammetry (CV) and differential pulse voltammetry (DPV) measurements, and present exciting opportunities for building electrochemical sensors using GQDs as probes [64]. Li *et al.* designed the first electrochemical sensors using GQDs based on the strong interaction between single-stranded DNA (ssDNA) and GQDs [60] (Fig. 7). The electrochemical platform designed was simple and smart, using GQD modified pyrolytic graphite electrodes coupled with specific sequence ssDNA molecules as probes. The probe ssDNA (ssDNA-1) can be easily immobilized thanks to the π–π stacking between the nucleobases and GQDs. The immobilized ssDNA inhibits the ET effect between the electro-active species $[Fe(CN)_6]^{3-/4-}$ and the electrode *via* electrostatic repulsion, resulting in a drastic decrease of the electrochemical signal. Once bound to the target molecules such as the target ssDNA (ssDNA-2) or target protein, the electrostatic repulsion of the electro-active species $[Fe(CN)_6]^{3-/4-}$ and the immobilized ssDNA is removed, the resulting peak currents increases. Razmi *et al.* introduced GQDs as a novel and suitable substrate for enzyme immobilization [61]. They immobilized glucose oxidase (GOx) on the GQD modified carbon ceramic electrode (CCE) and direct electrochemistry of GOx was realized. The developed biosensor responded efficiently and sensitively. The high performance of the

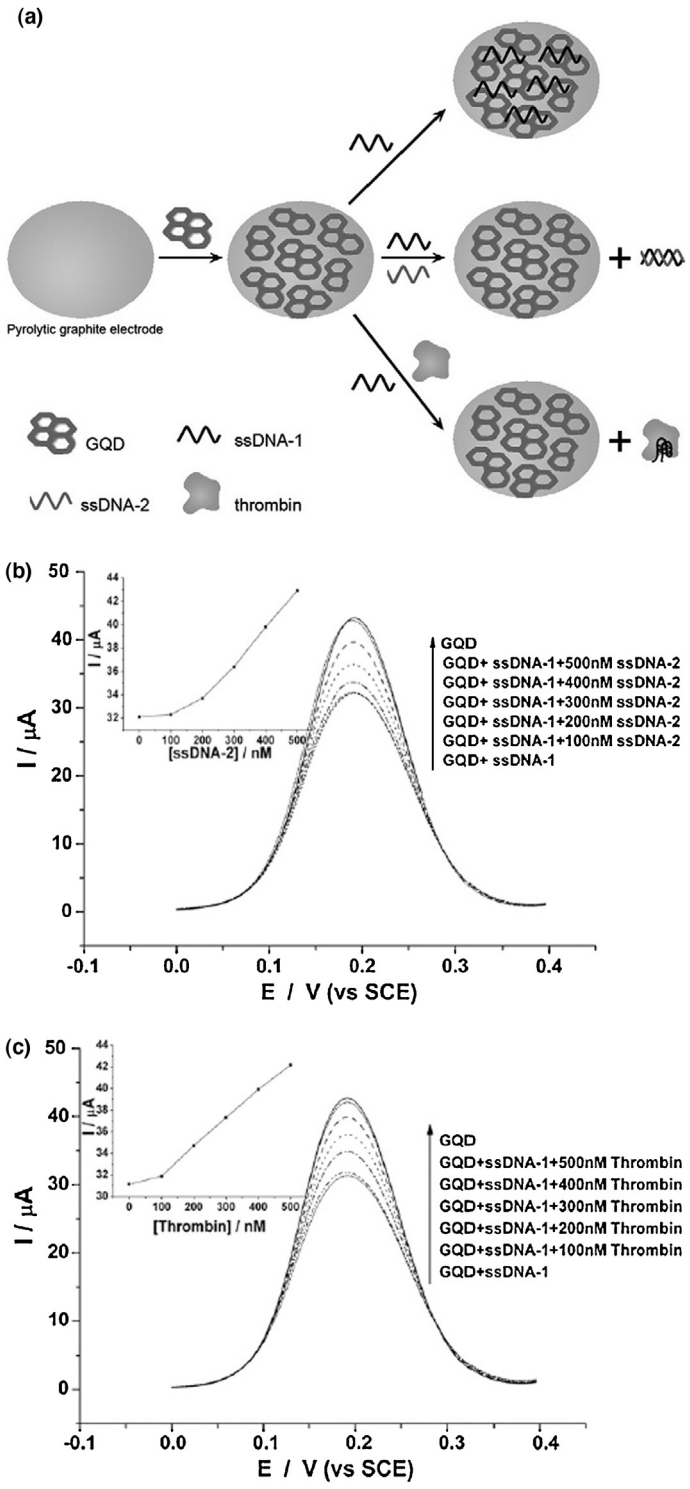

FIGURE 7

(a) Schematic illustration of different kinds of GQD-based electrochemical biosensors. DPVs for a 5 mM $[Fe(CN)_6]^{3-}/^{4-}$ in Tris–HCl buffer solution (pH 6.0, 10 mM) obtained at a GQD modified electrode with a ssDNA-1 (500 nM) probe were used to detect ssDNA-2 (b) and thrombin (c). Insets contain plots of the peak current against the concentration of ssDNA-2 (b) or thrombin (c). Reprinted with permission from [60]. © 2011 Elsevier.

biosensor was attributed to the large surface-to-volume ratio, excellent biocompatibility of the GQDs, and the abundance of hydrophilic edges, as well as the hydrophobic plane in GQDs which enhances the enzyme absorption on the electrode surface.

Ai and co-workers designed a novel sandwich-type electrochemical immunosensor with an Fe_3O_4@GQDs hybrid and apoferritin-encapsulated Cu (Cu-apoferritin) nanoparticles as labels for highly selective and sensitive detection of avian leukosis virus subgroup J (ALVs-J) [62]. The huge surface area of GQDs increased the loading of antibodies and Cu-apoferritin nanoparticles, and a large amount of electroactive probes could be captured by the apoferritin, which increased the electrochemical signal significantly and greatly increased the sensitivity of the immunosensor.

Our group first found that graphene oxide shows peroxidase-like activity [65]. GQDs, which are recognized as good electron transporters and acceptors, show similar peroxidase-like activity as well [63,66,67]. Guo and co-workers covalently assembled the GQDs with enriched periphery carboxylic groups on an Au electrode [63]. The GQDs showed highly peroxidase-like properties even after being assembled on Au; therefore, the as-prepared GQDs/Au electrode exhibited decent electrochemical catalytic properties toward the H_2O_2 decomposition. Electrochemical measurements reveal that the GQDs/Au electrode possesses a wide linear range, low detection limit, and fast amperometric response to H_2O_2. Moreover, the detection of H_2O_2 in living cells was realized by using this GQDs/Au electrode (Fig. 8).

Electrochemiluminescence sensors

Electrochemiluminescence (ECL), also referred to as electrogenerated chemiluminescence, a smart combination of chemiluminescence and electrochemistry, is a valuable detection method and becoming increasingly recognized in analytical chemistry due to its simplified set-up, label-free nature, low background signal and high sensitivity [68]. A series of semiconductor nanocrystals (also known as semiconductor QDs, CDs and silicon quantum dots), have been reported to show ECL emission properties, which show promise for the construction of ECL biosensors [68]. ECL emission is observed from GQDs as well [16,69]. When $S_2O_8^{2-}$ acts as a coreactant, strongly oxidizing $SO_4^{\bullet-}$ radicals and $GQDs^{\bullet-}$ anion radicals are produced by the electrochemical reduction of $S_2O_8^{2-}$ and GQDs, respectively, which shows an electrooxidation peak at −1.5 V (Fig. 9a). Subsequently, $SO_4^{\bullet-}$ radicals can react with $GQDs^{\bullet-}$ *via* electron-transfer annihilation, producing an excited state (GQDs*) that finally emits light. The possible ECL mechanisms are described by the following equations [16]:

$$GQDs + e^- \rightarrow GQDs^{\bullet-} \quad (1)$$

$$S_2O_8^{2-} + e^- \rightarrow S_2O_8^{\bullet 2-} \quad (2)$$

$$S_2O_8^{\bullet 2-} \rightarrow SO_4^{2-} + SO_4^{\bullet-} \quad (3)$$

$$GQDs^{\bullet-} + SO_4^{\bullet-} \rightarrow GQDs* + SO_4^{2-} \quad (4)$$

$$GQDs* \rightarrow GQDs + hv \quad (5)$$

When H_2O_2 works as coreactant, the electrooxidation of GQDs can produce the cation radicals, $GQDs^{\bullet+}$, which shows an electrooxidation peak at 0.4 V (Fig. 9b). HOO^- is oxidized to $O_2^{\bullet}$, while HOO^- is produced from the ionization balance of H_2O_2 in solution. The $O_2^{\bullet}$ radicals and $GQDs^{\bullet+}$ produced can lead to the formation of excited state GQDs*, and finally light is emitted.

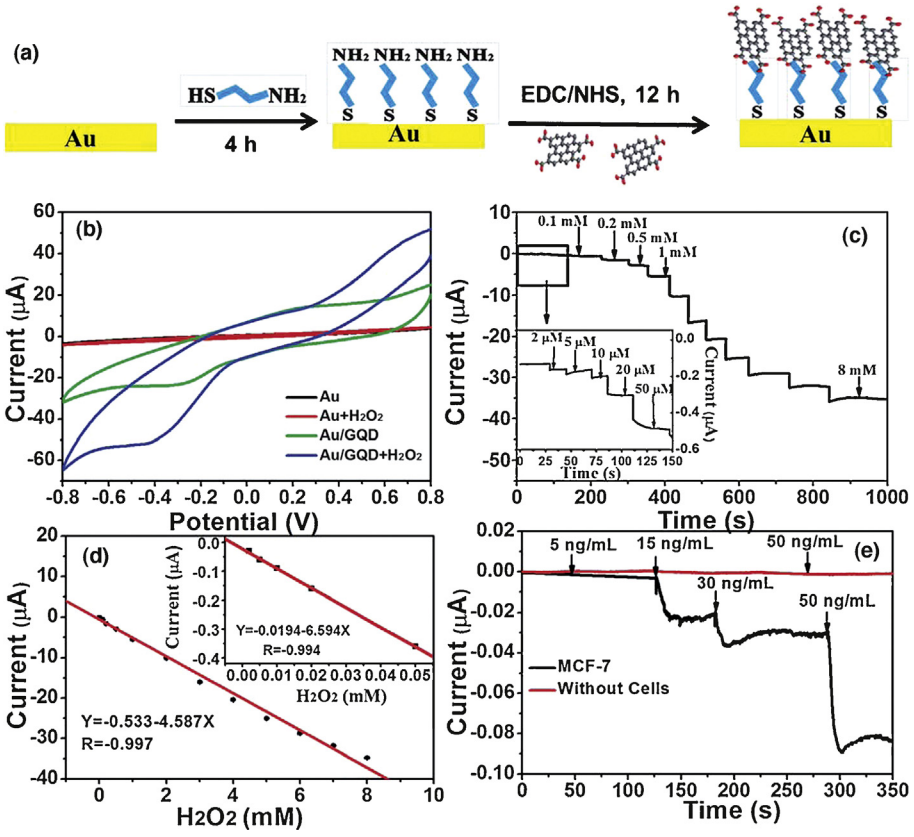

FIGURE 8

(a) Illustrative fabrication process of the GQDs/Au electrode, (b) CVs of the Au electrode, and GQD-modified Au electrode in oxygen-free PBS (0.01 M, pH 7) at a scan rate of 50 mV s^{-1}, (c) amperometric responses of the GQDs/Au electrode to the successive addition of H_2O_2 at an applied potential of −0.4 V. Inset contains an enlargement of the low concentration region, (d) standard amperometric responses of the GQDs/Au electrode to different H_2O_2 concentrations, (d) the progression of the H_2O_2 release from MCF-7 cells upon the addition of 5, 15, 30, and 50 ng mL^{-1} PMA. The red line represents the experiment without cells. Reprinted with permission from [63]. © 2013 The Royal Society of Chemistry.

The possible ECL process is described by the following equations [69]:

$$GQDs - e^- \rightarrow GQDs^{\bullet +} \quad (6)$$

$$H_2O_2 \rightleftarrows H^+ + HOO^- \quad (7)$$

$$HOO^- - e^{\bullet -} \rightarrow HOO^{\bullet} \leftrightarrow O_2^{\bullet} \quad (8)$$

$$GQDs^{\bullet +} + O_2^{\bullet} \rightarrow GQDs* \quad (9)$$

$$GQDs* \rightarrow GQDs + hv \quad (10)$$

ECL emission was observed from the as-prepared GQDs by Zhu and co-workers for the first time [16]. The GQDs were demonstrated to possess negligible surface defects, as suggested by the tiny red-shift between their PL and ECL spectra [16]. A novel ECL

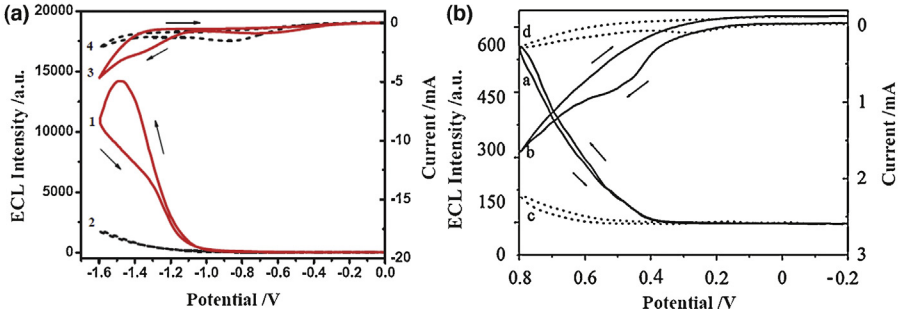

FIGURE 9

(a) ECL–potential curves and cyclic voltammograms (CVs) of the GQDs (1, 3) and background (2, 4) with concentration of 20 ppm in 0.05 M Tris–HCl (pH 7.4) buffer solution containing 0.1 M $K_2S_2O_8$. Scan rate: 100 mV s^{-1}. Reprinted with permission from [16]. © 2012 Wiley-VCH Verlag GmbH & Co. KGaA and (b) ECL–potential curves and CV of the GQDs in 0.1 M, pH 7.4 PBS in the presence (solid line) and absence (dotted line) of 5 mM H_2O_2. Reprinted with permission from [69]. © 2013 Elsevier.

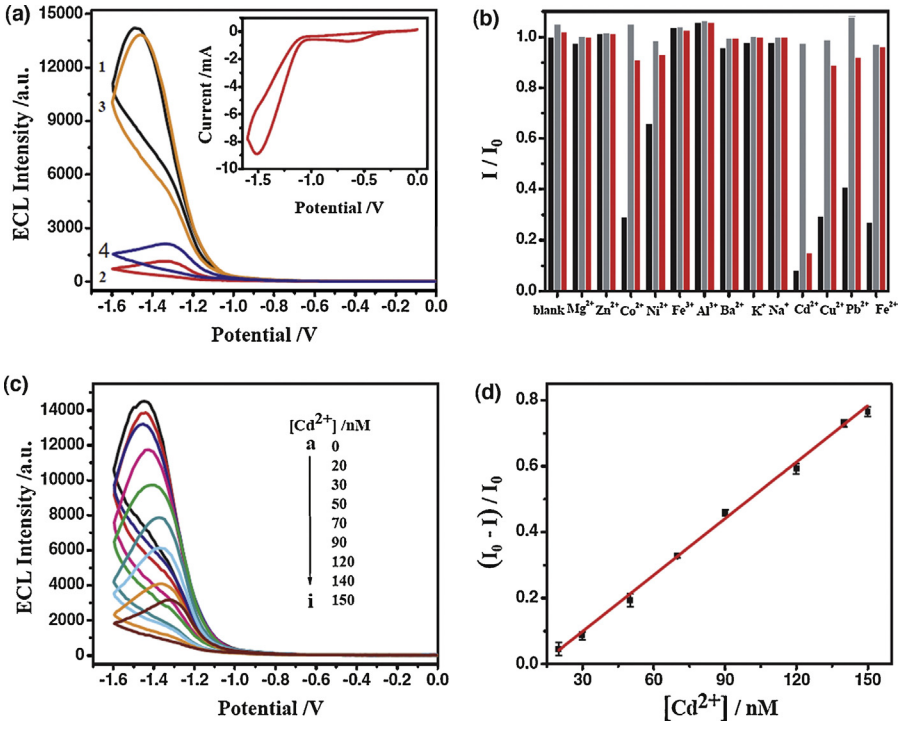

FIGURE 10

(a) ECL–potential curves of the GQDs (1), the GQDs with the addition of 20 μM Cd^{2+} (2), the GQDs with the successive addition of 20 μM Cd^{2+}, 40 μM EDTA (3), or 1 mM Cys (4) in 0.05 M, pH 7.4 TBS with 0.1 M $K_2S_2O_8$. Inset: CV corresponds to (2), (b) the selective of various metal ions (20 μM), (c) ECL–potential curves of GQDs in the presence of different concentrations of Cd^{2+} .The electrolyte is 0.05 M, pH 7.4 TBS with 0.1 M $K_2S_2O_8$ and 1 mM Cys, and (d) linear calibration plot for Cd^{2+} detection. Reprinted with permission from [16]. © 2012 Wiley-VCH Verlag GmbH & Co. KGaA.

sensor for Cd^{2+} was proposed based on the competitive coordination between cysteine (Cys) and GQDs for metal ions (Fig. 10). Using H_2O_2 as coreactant, Yu *et al.* developed an ECL aptamer sensor measuring ATP [69]. Furthermore, as an amplified element, SiO_2/GQD composites were used to produce an amplified ECL signal and improve the sensitivity of the sensor. The proposed ECL aptamer sensors had high sensitivity, good precision, acceptable stability, reproducibility, and sensitivity. In summary, ECL active GQDs are expected to have promising applications in the development of novel ECL biosensors due to their low cytotoxicity, low cost, excellent solubility, and ease of labeling [16,69].

Conclusions and future perspectives

In this review, we have summarized the advantages of GQDs-based sensors. Significant progress has been made in the design of novel sensors based on the excellent properties of GQDs, and been applied in different fields. We have discussed electronic sensors, PL sensors, electrochemical sensors and electrochemiluminescence sensors of GQDs which have been applied to physical analysis, chemical analysis and bioanalysis. Although GQDs have attracted tremendous research interest, research on GQDs is still in its initial stage, especially in the field of GQD based sensors; most of the references in this review have appeared in the last 2 years. Moreover, the low product yield and QY, the confusing relationship between the surface chemistry and physicochemical properties has restricted the performance of GQDs for sensing. Thus, there is a huge development space for GQDs. Considering the unique properties of GQDs and the current challenges for developing smart sensors, our perspectives on GQDs based sensors in the near future are as follows:

Sensors based on the upconversion PL of GQDs

Two-photon fluorescence imaging or upconversion fluorescence imaging, with advantages including a larger penetration depth, a minimized tissue auto fluorescence background, the avoidance of harmful UV or blue excitations and the reduction of photodamage in biotissues, has received a great deal of attention for its promising applications in both basic biological research and clinical diagnostics [15]. What's more, short-wavelength UV or visible light does not penetrate very far into tissue, which limits its utility for deep tissue imaging [70]. Some GQDs have been reported to possess upconversion PL properties [1–4]. Gong and co-workers prepared N-GQDs using a one-pot solvothermal approach using DMF as a solvent and nitrogen source. The resulting N-GQDs exhibited a two-photon absorption cross section and were demonstrated to be an efficient two-photon fluorescent probe for cellular and deep tissue imaging [15]. Thus, upconversion PL will prompt the use of GQDs as a tool in many kinds of biomedical applications, such as deep tissue and *in vivo* sensing.

Surface-enhanced Raman spectroscopy (SERS) sensors based on GQDs

Surface-enhanced Raman spectroscopy (SERS) is expected to have a major impact as a sensitive analytical technique and tool for fundamental studies of surface species [71]. The well-organized assembly of zero dimensional (0D) GQDs into 1D nanotube (NT)

arrays, and their significant potential as a new metal-free platform for efficient SERS applications have been reported [72]. The emergence of GQD NTs can be used to reduce the substantial cost of SERS sensors by using low-cost carbon materials instead of expensive noble metal substrates.

Quantum yield improvement of GQDs

The intensity of PL is very important for a PL sensor. Unfortunately, like CDs, the QY of GQDs is usually very low [1–4]. Therefore, the preparation of GQDs with a high QY is demanding and important. To this end, many methods for modulating the fluorescence emission spectra of GQDs and improving its QY have been reported. Zhu *et al.* used $NaBH_4$ as reducing agent to convert greenish-yellow luminescent GQDs synthesized through a microwave assisted method, to bright blue luminescent GQDs with a higher QY [16]. Our group reported that the luminescence of GQDs was greatly enhanced by increasing sp^2 domains and electron-donating groups in GQDs through photochemical reduction and the hydrothermal method [38,39]. Up to now, even the highest QY of GQDs is 73% [42], the QY of most GQDs ranges from 2 to 22.9% [3,4], which is much lower than that semiconductive QDs [73]. The QY improvement of GQDs is challenging for their practical applications and requires a great deal of devoted effort.

Acknowledgments

Financial support was provided by 973 project (2011CB936004) and NSFC (21210002 and 91213302).

References

[1] J.H. Shen, et al. Chem. Commun. 48 (2012) 3686.
[2] S.J. Zhu, et al. Chem. Commun. 48 (2012) 4527.
[3] Z.P. Zhang, et al. Energy Environ. Sci. 5 (2012) 8869.
[4] L. Li, et al. Nanoscale 5 (2013) 4015.
[5] L.A. Ponomarenko, et al. Science 320 (2008) 356.
[6] L.J. Wang, et al. Appl. Phys. Lett. 97 (2010) 262113.
[7] S. Fringes, et al. Phys. Status Solidi B 248 (2011) 2684.
[8] J. Guettinger, et al. Phys. Rev. B 83 (2011) 165445.
[9] T. Mueller, et al. Appl. Phys. Lett. 101 (2012) 12104.
[10] J. Peng, et al. Nano Lett. 12 (2012) 844.
[11] Y.Q. Dong, et al. J. Mater. Chem. 22 (2012) 8764.
[12] D.Y. Pan, et al. Adv. Mater. 22 (2010) 734.
[13] H. Tetsuka, et al. Adv. Mater. 24 (2012) 5333.
[14] D.Y. Pan, et al. J. Mater. Chem. 22 (2012) 3314.
[15] Q. Liu, et al. Nano Lett. 13 (2013) 2436.
[16] L.L. Li, et al. Adv. Funct. Mater. 22 (2012) 2971.
[17] S. Chen, et al. Chem. Commun. 48 (2012) 7637.
[18] S.J. Zhuo, et al. ACS Nano 6 (2012) 1059.
[19] Y. Li, et al. Adv. Mater. 23 (2011) 776.
[20] Y. Li, et al. J. Am. Chem. Soc. 134 (2012) 15.
[21] M. Zhang, et al. J. Mater. Chem. 22 (2012) 7461.
[22] D.B. Shinde, V.K. Pillai, Chem. Eur. J. 18 (2012) 12522.
[23] X.J. Zhou, et al. ACS Nano 6 (2012) 6592.
[24] T. Gokus, et al. ACS Nano 3 (2009) 3963.
[25] F. Liu, et al. Adv. Mater. 25 (2013) 3657.
[26] L.X. Lin, S.W. Zhang, Chem. Commun. 48 (2012) 10177.
[27] X. Yan, et al. J. Am. Chem. Soc. 132 (2010) 5944.
[28] Q. Li, et al. J. Am. Chem. Soc. 134 (2012) 18932.
[29] X. Yan, et al. Nano Lett. 10 (2010) 1869.
[30] L.B. Tang, et al. ACS Nano 6 (2012) 5102.
[31] Y.Q. Dong, et al. Carbon 50 (2012) 4738.
[32] J. Lu, et al. Nat. Nanotechnol. 6 (2011) 247.
[33] R.L. Liu, et al. J. Am. Chem. Soc. 133 (2011) 15221.
[34] S. Kim, et al. ACS Nano 6 (2012) 8203.
[35] T. Ihn, et al. Mater. Today 13 (2010) 44.
[36] T.S. Sreeprasad, et al. Nano Lett. 13 (2013) 1757.
[37] F. Yang, et al. J. Mater. Chem. 22 (2012) 25471.
[38] H.J. Sun, et al. ACS Appl. Mater. Interfaces 5 (2013) 1174.
[39] H.J. Sun, et al. Chem. Eur. J. 19 (2013) 13362.
[40] C.F. Hu, et al. J. Mater. Chem. B 1 (2013) 39.
[41] M. Li, et al. Appl. Phys. Lett. 101 (2012) 103107.
[42] Y.Q. Dong, et al. Angew. Chem. Int. Ed. 52 (2013) 7800.
[43] K. Lingam, et al. Adv. Funct. Mater. 23 (2013) 5062.
[44] G. Eda, et al. Adv. Mater. 22 (2010) 505.
[45] K.P. Loh, et al. Nat. Chem. 2 (2010) 1015.
[46] D. Wang, et al. Carbon 50 (2012) 2147.
[47] Y. Dong, et al. Anal. Chem. 84 (2012) 8378.
[48] L. Fan, et al. Talanta 101 (2012) 192.
[49] J.M. Bai, et al. Chem. Eur. J. 19 (2013) 3822.
[50] Y.H. Li, et al. Chem. Commun. 49 (2013) 5180.
[51] J.J. Liu, et al. Nanoscale 5 (2013) 1810.
[52] X. Ran, et al. Chem. Commun. 49 (2013) 1079.
[53] H. Zhao, et al. Chem. Commun. 49 (2013) 234.
[54] D. Liu, et al. Chem. Commun. 49 (2013) 2503.
[55] H. Chakraborti, et al. Mater. Lett. 97 (2013) 78.
[56] G. He, et al. ACS Catal. 3 (2013) 831.
[57] W.W. Liu, et al. Adv. Funct. Mater. 23 (2013) 4111.
[58] W.W. Liu, et al. Nanoscale 5 (2013) 6053.
[59] V. Gupta, et al. J. Am. Chem. Soc. 133 (2011) 9960.
[60] J. Zhao, et al. Electrochem. Commun. 13 (2011) 31.
[61] H. Razmi, R. Mohammad-Rezaei, Biosens. Bioelectron. 41 (2013) 498.
[62] X. Wang, et al. Biosens. Bioelectron. 47 (2013) 171.
[63] Y. Zhang, et al. Nanoscale 5 (2013) 1816.
[64] D.B. Shinde, V.K. Pillai, Angew. Chem. Int. Ed. 52 (2013) 2482.
[65] Y.J. Song, et al. Adv. Mater. 22 (2010) 2206.
[66] F. Jiang, et al. Nanoscale 5 (2013) 1137.
[67] J.X. Zhao, et al. J. Mater. Chem. C 1 (2013) 4676.
[68] L. Wu, et al. Chem. Commun. 49 (2013) 5675.
[69] J. Lu, et al. Biosens. Bioelectron. 47 (2013) 271.
[70] J. Zhou, et al. Chem. Soc. Rev. 41 (2012) 1323.
[71] J.P. Camden, et al. Acc. Chem. Res. 41 (2008) 1653.
[72] H. Cheng, et al. ACS Nano 6 (2012) 2237.
[73] D.V. Talapin, et al. Chem. Rev. 110 (2010) 389.